Solution Conformation of the Antibody-Bound Tyrosine Phosphorylation Site of the Nicotinic Acetylcholine Receptor β-Subunit in Its Phosphorylated and Nonphosphorylated States†

Angélique Phan-Chan-Du,‡ Christine Hemmerlin,‡ Dimitrios Krikorian,§ Maria Sakarellos-Daitsiotis,§ Vassilios Tsikaris,§ Constantinos Sakarellos,§ Martha Marinou,|| Aurélien Thureau,‡ Manh Thong Cung,*,‡ and Socrates J. Tzartos*,||,⊥

Laboratoire de Chimie-Physique Macromoléculaire, UMR 7568 CNRS−INPL, Groupe ENSIC, 1 Rue Grandville, B.P. 451, 54001 Nancy Cedex, France, Department of Chemistry, University of Ioannina, Box 1186, 451 10 Ioannina, Greece, Department of Biochemistry, Hellenic Pasteur Institute, 127 Vassilissis Sofias Avenue, 115 21 Athens, Greece, and Department of Pharmacy, University of Patras, 265 04 Patras, Greece

Received February 7, 2003

ABSTRACT: Phosphorylation of the acetylcholine receptor (AChR) seems to be responsible for triggering several effects including its desensitization and aggregation at the postsynaptic membrane and probably initiates a signal transduction pathway at the postsynaptic membrane. To study the structural and functional role of the tyrosine phosphorylation site of the AChR β-subunit and contribute to the in-depth understanding of the structural basis of the ion channel function, we synthesized four peptides containing the phosphorylated and nonphosphorylated sequences (380−391) of the human and *Torpedo* AChR β-subunits and studied their interaction with a monoclonal antibody (mAb 148) that is known to bind to this region and that is capable of blocking ion channel function. All four peptides were efficient inhibitors of mAb 148 binding to AChR, although the nonphosphorylated human peptide was considerably less effective than the three others. We then investigated the conformation acquired by all four peptides in their antibody-bound state, which possibly illustrates the local conformation of the corresponding sites on the intact AChR molecule. The phosphorylated human and *Torpedo* peptides adopted a distorted 3_{10} helix conformation. The nonphosphorylated *Torpedo* peptide, which is also an efficient inhibitor, was also folded. In contrast, the nonphosphorylated human peptide (a less efficient inhibitor) presented an extended structure. It is concluded that the phosphorylation of the AChR at its β-subunit Tyr site leads to a significant change in its conformation, which may affect several functions of the AChR.

The nicotinic acetylcholine receptor (AChR)[1] from fish electric organs and vertebrate skeletal muscles is a transmembrane glycoprotein composed of five homologous subunits in the stoichiometry $\alpha_2\beta\gamma\delta$ or $\alpha_2\beta\epsilon\delta$, forming the cation channel (*1*, *2*). Each subunit consists of a large N-terminal extracellular domain (about half the subunit), four transmembrane segments, M1-M4, a large cytoplasmic domain between M3 and M4, and a short C-terminal extracellular tail. The pore of the molecule is formed by a pentameric bundle of M2 helices, one M2 helix from each subunit forming the cation channel. The five M2 helices are clustered in the middle of the membrane, forming the channel gate. In its resting state, the gate is impermeable to ions but opens when ACh binds to distant sites on the two α-subunits and closes when ACh is removed from the synaptic cleft or when desensitization occurs (*3*). A set of narrow openings between the subunits at the cytoplasmic wall of the channel, through which ions can flow, has been recently described

† This work was supported by the Association Française contre les Myopathies (AFM), the Biotechnology program of the EU (Grant BIO4-CT98-0110), the Quality of Life program of the EU (Grant QLG3-CT-2001-00902), and the Centre National de la Recherche Scientifique.

* To whom correspondence should be addressed. (M.T.C) Phone: (33) 383 175107. Fax: (33) 383 379977. E-mail: Manh-Thong.Cung@ensic.inpl-nancy.fr. (S.J.T.) Phone: 30-210-6478844. Fax: 30-210-6478842. E-mail: tzartos@mail.pasteur.gr.

‡ Laboratoire de Chimie Physique Macromoléculaire.

§ University of Ioannina.

|| Hellenic Pasteur Institute.

⊥ University of Patras.

[1] Abbreviations: ACh, acetylcholine; AChR, nicotinic acetylcholine receptor; Boc, *tert*-butyloxycarbonyl; BSA, bovine serum albumin; CVFF, consistent-valence force field; DCM, dichloromethane; DG, distance geometry calculations; DIEA, diisopropylethylamine; DMF, dimethylformamide; ELISA, enzyme-linked immunosorbent assay; EM, energy minimization; Fmoc, 9-fluorenylmethyloxycarbonyl; ES-MS, electrospray mass spectrometry; HF, hydrogen fluoride; HOBt, 1-hydroxybenzotriazole; HPLC, high performance liquid chromatography; mAb, monoclonal antibody; MD, molecular dynamics; MG, myasthenia gravis; MIR, main immunogenic region; NOESY, nuclear Overhauser enhancement spectroscopy; Pam resin, 4-hydroxymethylphenylacetamido methylpolystyrene; Pbf, 2,2,4,6,7-pentamethyl-dihydrobenzofuran-5-sulfonyl; PBS, phosphate-buffered saline; RIA, radioimmunoassay; rmsd, root-mean-square deviation; SA, dynamical simulated annealing; SDS, sodium dodecyl sulfate; TBTU, 2-(1*H*-benzotriazol-1-y1)-1,1,3,3-tetramethyluronium tetrafluoroborate; TFA, trifluoroacetic acid; TIS, triisopropylsilane; TMPS-d_4, tetradeutero 2,2,3,3-(trimethylsilyl)-3-propionic acid sodium salt; TPPI, time proportional phase incrementation; TOCSY, total correlation spectroscopy; TR-NOE, transferred nuclear Overhauser enhancement; VICE, very immunogenic cytoplasmic epitope; Wang resin, *p*-benzyloxybenzyl alcohol resin (HMP, Wang-type); WATERGATE, water suppression by gradient-tailored excitation.

10.1021/bi030034u CCC: $25.00
Published on Web 05/30/2003

(*4*). Despite the available information, the functional mechanism of the AChR is not yet clearly understood.

Monoclonal antibodies (mAbs) against the cytoplasmic region of the AChR can be elicited by immunization with denatured AChR; the precise epitopes for many of these mAbs have been identified, making them useful markers in many localization studies (*5*). In particular, the very immunogenic cytoplasmic epitopes on the α- and *β*-subunits (VICE-α and VICE-*β*) have been localized to the α373−380 and *β*381−388 (consensus sequencing) regions and are of special interest, respectively, in myasthenia gravis (MG), an autoimmune disease caused by anti-AChR antibodies, and in AChR phosphorylation (*6, 7*).

Protein phosphorylation is intimately involved in the regulation of synaptic function (*8*). Phosphorylation of the AChR seems to trigger several effects (*9*). The AChR is phosphorylated by at least three protein kinases, and the phosphorylation sites contain five serine and three tyrosine residues. The *β*Tyr384 phosphorylation site in both the human and the *Torpedo β*-subunits is part of VICE-*β* (*10*).

Phosphorylation of the AChR increases its desensitization rate, mediates its aggregation at postsynaptic membranes, and probably initiates a signal transduction pathway at the postsynaptic membrane (*9, 11*−*15*). In addition, single mAbs to epitopes containing the *β*- or *γ*-subunit tyrosine phosphorylation sites (*β*Tyr384, *γ*Tyr385) efficiently inhibit the agonist-induced opening of the ion channel, suggesting that each of these sites is capable of controlling the channel (*16*−*19*). It has been shown that tyrosine phosphorylation of the *β*-subunit of the intact AChR remarkably reduces VICE-*β* mAb binding to the AChR (including the blocker of AChR function mAb 148) (*10*).

To investigate the structural and functional role of the tyrosine phosphorylation site of the AChR *β*-subunit and to contribute to the in-depth understanding of the structural basis of the ion channel function, four peptides containing the phosphorylated and nonphosphorylated VICE-*β* sequence (380−391) of the human and *Torpedo* AChR were synthesized. A series of mAbs that interact with the VICE-*β* region of the AChR (*10*) was tested for binding to these peptides. The mAb 148, which is known to block the ion channel (*16, 17*) and bind well to both nonphosphorylated and phosphorylated peptides, was selected for further study.

The complete conformational study, by NMR, of an intact antibody, with its bound antigen, is not feasible because of the large size of such a complex. However, for binding ligands, a NMR approach, developed by Clore and Gronenborn (*20, 21*) is successfully applied to investigate the conformation of a ligand in its bound form. This approach, usually referred to as transferred nuclear Overhauser enhancement (TR-NOE) spectroscopy, relies on the measurement of magnetization transfer between protons that are close in space. For such protons belonging to a small unbound ligand, which is rapidly tumbling in solution, the magnetization transfer rate is very slow as compared to the very fast transfer rate observed for protons of a ligand bound to a very large molecule, such as an antibody, that is slowly tumbling. The TR-NOE approach has been now widely applied in determining the conformations of a wide range of small ligands in the protein-bound state by focusing on the easily detected NMR signals of the free ligands (*22*−*26*). In the present study, we carried out 2-D TR-NOESY and molecular dynamics simulation to determine the structural properties of the four synthesized peptides, when bound to mAb 148. The relationship between the structural features of the mAb 148-bound phosphorylated or nonphosphorylated peptides and their ability to inhibit the binding of mAbs to AChR is also discussed in regard to the local conformation of the phosphorylation site of the intact AChR.

MATERIALS AND METHODS

Reagents. 2-(1*H*-Benzotriazol-1-y1)-1,1,3,3-tetramethyluronium tetrafluoroborate (TBTU), 1-hydroxybenzotriazole (HOBt), *tert*-butyloxycarbonyl (Boc)- and 9-fluorenylmethyloxycarbonyl (Fmoc)-protected amino acids, and sodium dodecyl sulfate (SDS) were obtained from Bachem Biochemica GmbH (Germany) and Neosystem Laboratoire (France). Solvents were from Labscan Ltd. (Ireland) and were used without further purification, while trifluoroacetic acid (TFA), diisopropylethylamine (DIEA), and piperidine were purchased from Merck Schuchardt (Germany). Boc-*β*-Ala-Pam and Fmoc-Gly-Wang resins were from Calbiochem-Novabiochem GmbH (Germany). High performance liquid chromatography (HPLC) grade acetonitrile was purchased from Merck Darmstadt (Germany).

Solid-Phase Synthesis of the Human and Torpedo 380−*391 Sequences Containing the βTyr384 AChR Phosphorylation Site.* Because of the presence of proline at the penultimate C-terminal position of the human peptide sequence, a *β*-Ala residue was initially introduced as a spacer to avoid the formation of diketopiperazine and loss of the peptide from the resin (*27*, *28*). However, the relatively low yield of the peptide G^{380}TDEYFIRKPPS^{391}*β*-Ala after cleavage from the Pam resin prompted us to use glycine instead of *β*-Ala and thus the Fmoc-Gly-Wang resin for starting the synthesis of the phosphorylated peptide.

Human G^{380}TDEYFIRKPPS^{391}β-Ala. The synthesis was carried out manually by using Boc-chemistry, stepwise solid-phase synthesis procedure (*29*−*31*), and Pam resin (0.13 mmol/g resin). Aspartic and glutamic residues were introduced, as Boc-Asp(OBzl)-OH and Boc-Glu(OBzl)-OH, respectively, tyrosine as Boc-Tyr (2,6-diCl−Bzl)-OH, arginine as Boc-Arg(Tos)-OH, lysine as Boc-Lys(Fmoc)-OH, and threonine and serine, as Boc-Thr(Bzl)-OH and Boc-Ser(Bzl)-OH, respectively.

The Boc groups were removed by 40% TFA in dichloromethane (DCM), and the resulting salt was neutralized with DIEA. Couplings were performed using an amino acid/TBTU/HOBt/DIEA/resin molar ratio of 3:2.9:3:3:1. Deprotection and coupling reactions were monitored using the Kaiser test. The crude peptide was cleaved from the resin using hydrogen fluoride (HF) in the presence of anisole and phenol as scavengers. After precipitation with cold ethyl ether, the material was extracted using aqueous acetic acid (2 N), lyophilized (yield 40%), and then subjected to preparative reverse phase HPLC using a C18 column (solvent A, H_2O/0.1% TFA; solvent B, CH_3CN/0.1% TFA, programmed gradient 90:10−70:30), the final yield of the purified peptide being 10%. The purity of the peptide was checked by analytical HPLC, and the molecular mass was confirmed as correct by electrospray mass spectrometry (ES-MS) (expected M^+: 1481.65, found M^+: 1481.16).

Human G^{380}TDEY(PO$_3$H$_2$)FIRKPPS^{391}G. The synthesis was carried out manually using Fmoc-chemistry, stepwise

solid-phase synthesis procedure (*29*−*31*), and Fmoc-Gly-Wang resin (0.8 mmol/g resin). Aspartic and glutamic acids were introduced, as Fmoc-Asp-(OtBu)-OH and Fmoc-Glu-(OtBu)-OH, respectively, tyrosine as Fmoc-Tyr (PO_3H_2)-OH (*32*), arginine as Fmoc-Arg(Pbf)-OH (Pbf: 2,2,4,6,7-pentamethyl-dihydrobenzofuran-5-sulfonyl), lysine as Fmoc-Lys-(Boc)-OH, and threonine and serine, as Fmoc-Thr(tBu)-OH and Fmoc-Ser(tBu)-OH, respectively.

Fmoc groups were removed using 40% piperidine in dimethylformamide (DMF). Couplings were performed using an amino acid/TBTU/HOBt/DIEA/resin molar ratio of 3:2.9:3:3:1. DMF, used for couplings, was previously distilled to remove traces of amines. Deprotection and coupling reactions were monitored by the Kaiser test. The crude peptide was obtained by treatment of the peptidyl resin for 2.5 h with a mixture of TFA/TIS/water (90:5:5) (TIS/triisopropylsilane), which does not cause dephosphorylation of the peptide (*33*). The resin was removed by filtration, the filtrate was evaporated under reduced pressure, and the product precipitated with cold ethyl ether (yield ~80%). The peptide was then purified by preparative reverse phase HPLC on a C18 column (solvent A, H_2O/0.1% TFA; solvent B, CH_3CN/0.1% TFA, programmed gradient 90:10−40:60) with a final yield of ~42%. The purity of the peptide was checked by analytical HPLC, and the molecular mass was confirmed as correct by ES-MS (expected M^+: 1548.16, found M^+: 1547.32).

Torpedo A^{380}NDEYFIRKPAG^{391}. The synthesis was carried out using Fmoc-Gly-Wang resin (0.8 mmol/g resin) as above. Aspartic and glutamic residues were introduced, as Fmoc-Asp-(OtBu)-OH and Fmoc-Glu-(OtBu)-OH, respectively, asparagine as Fmoc-Asn-(Trt)-OH (Trt: trityl group), arginine as Fmoc-Arg(Pbf)-OH, and tyrosine as Fmoc-Tyr(tBu)-OH. The yield of the crude peptide after cleavage from the resin was 76%. The peptide was purified by preparative reverse phase HPLC (solvent A, H_2O/0.1% TFA; solvent B, CH_3CN/0.1% TFA, programmed gradient 95:5−30:70) with a yield of 20%. The purity of the peptide was checked by analytical HPLC, and the molecular mass was confirmed as correct by ES-MS (expected M^+: 1381.53, found M^+: 1381.03).

Torpedo A^{380}NDEY(PO_3H_2)FIRKPAG^{391}. The synthesis was carried out using Fmoc-Gly-Wang resin (0.8 mmol/g resin), as above, using Fmoc-Tyr(PO_3H_2)-OH instead of Fmoc-Tyr(tBu)-OH. The yield of crude peptide was 60%. The peptide was purified by preparative HPLC (solvent A, H_2O/0.1% TFA; solvent B, CH_3CN/0.1%TFA, programmed gradient 95:5−30:70) with a yield of ~18%. The molecular mass was confirmed as correct by ES-MS (expected M^+: 1461.51, found M^+: 1460.77).

Monoclonal Antibodies. The characteristics of the mAbs used for the binding assays, produced from rats immunized with *Torpedo* AChR, have been described previously (*10*, *34*, *35*). Except for the control mAbs, all of the mAbs used had been previously shown, using Pepscan peptides, to be directed against region β383−389 of the *Torpedo* AChR (*10*). mAb 148 was produced in large quantities as serum-free culture supernatants that were concentrated 100−200-fold, dialyzed, and used in the following NMR experiments.

ELISA Assessment of mAb Binding to Peptides. Wells of microtiter plates (MaxiSorp F96, Nunc) were coated by overnight incubation at 4 °C with 1 μg of peptide in 100 μL of 50 mM carbonate buffer, pH 9.6. The coated wells were washed three times with phosphate-buffered saline (PBS), pH 7.5, then saturated by incubation for 1 h at room temperature with 200 μL of 2.5% BSA in PBS. After three PBS washes, dilutions (1:200 and 1:1000) of mAb in 100 μL of PBS, 0.2% BSA were added to the wells, and the plates were incubated for 2 h at room temperature**.** After three washes with PBS, 0.05% Tween and three washes with PBS, 100 μL of peroxidase-conjugated rabbit anti-rat Ig antibody (Dako A/S, Denmark) (dilution 1:500) in PBS, 0.2% BSA was added for 1.5 h at room temperature. After three washes with PBS, 0.05% Tween and three washes with PBS, bound mAb was detected by measuring peroxidase activity, using 2,2′-azino-bis (3-ethylbenzothiazoline-6-sulfonic acid) as substrate, the color developed after about 20 min being measured at 405 nm using a microtiter plate reader.

Radioimmunoassay (RIA). The selected antibodies were used in a competitive soluble-phase RIA assay in which the peptides were tested for their ability to inhibit the binding of mAbs to the AChR. Homogenized AChR-rich *Torpedo* electric organ membranes were labeled by a 2 h preincubation with ^{125}I-α-bungarotoxin (added at an equimolar ratio), washed, solubilized using 0.5% Triton X-100 in PBS, pH 7.5, and centrifuged to precipitate any nonsolubilized material; the extract, containing labeled AChR, was used in the RIA. Each mAb (at a concentration capable of precipitating about 70% of the AChR) was incubated overnight at 4 °C with various concentrations of peptides or medium alone, then 0.2 pmol of ^{125}I-α-bungarotoxin-labeled *Torpedo* AChR was added per reaction tube, and the mixture was incubated for 3 h at 4 °C. The complexes formed were immunoprecipitated by incubation for 1.5 h at 4 °C with rabbit anti-rat immunoglobulin serum, the precipitates washed twice with PBS, 0.5% Triton X-100, and the precipitated radioactivity counted. The percent inhibition of mAb binding was calculated based on the amount of radioactivity precipitated in the presence and absence of peptide.

^{1}H NMR Experiments. D_2O (99.8%) and tetradeutero 2,2,3,3-(trimethylsilyl)-3-propionic acid sodium salt (TMPS-d_4) were purchased from Euriso-top (France). The nonphosphorylated or phosphorylated peptides and mAb 148 were dissolved at a molar ratio of 50:1 (i.e., 2.5 mM peptide and 0.05 mM mAb) in H_2O/D_2O (95:5 v/v) at pH 7.0 (100 mM phosphate buffer containing 0.02% sodium azide and TMPS-d_4 as an internal reference). These conditions led to intense, negative transferred NOESY cross-peaks assigned to the mAb-bound antigen (*36*). Spectra were recorded at 4 °C using a Bruker DRX600 NMR spectrometer. 2-D total correlated spectroscopy (TOCSY) was performed on each peptide with a mixing time, τ_m, of 70 ms. Four 2-D-NOESY experiments with mixing times ranged from 100 to 500 ms were performed. The buildup curve (*37*) for different NOE correlations showed that spin diffusion was negligible for $\tau_m = 200$ ms. The spectral width in F1 was 6600 Hz. Water resonance suppression in the TOCSY and NOESY experiments was achieved using the WATERGATE sequence (*38*, *39*). Data processing was performed using XWIN NMR software. The intensity of the peaks was extracted from the NOESY spectra ($\tau_m = 200$ ms) using XEASY software (*40*), and the interproton distances were calculated taking as reference the distance of 1.78 Å between the two Asp-C$^\beta$H$_2$ protons. Distance restraints were classified as strong, me-

dium, and weak and set as intervals of 1.8−2.5, 2.5−3.5, and 3.5−5.5 Å, respectively.

Molecular Dynamics Calculation. Energy minimization (EM) and molecular dynamics (MD) calculations were performed on an Octane Silicon Graphics workstation. Calculations of a set of 100 initial random structures were carried out first using DYANA-1.4 (*41*) program with 10 000 steps of simulated annealing (SA) from the temperature of 8−0 units (measured in target function units). SA, which involved the exploration of the maximum conformational space to find the global minimum energy conformation of the molecule, has been shown to be a useful procedure for the study of constrained systems (*42*−*44*). Refinement with restrained minimization was performed on the structures (50−70 structures) having the lowest energies. Each of them was then submitted to 900 steps of minimization (300 steps steepest descent, 300 steps conjugate gradient, and 300 steps Newton−Raphson method), 35 ps of MD in vacuo at 300 K for equilibration and finally 200 ps of MD applying derived NMR restraints with a force constant of 20 kcal mol^{-1} $Å^{-2}$. Conjugate gradient EM was completed within 750 steps. Refined structures were clustered into families and evaluated in regard to their stereochemical qualities using MOLMOL-2.5.1 software (*45*).

For MD and EM calculations, the DISCOVER-3 module from MSI software (Molecular Simulations Inc., San Diego, CA) was used. The consistent valence force field (CVFF) with a default cutoff distance of 9.5 Å and a distance-dependent dielectric constant equal to 4*r* was applied to all peptides (*46*). To avoid structural artifacts because of overestimation of Coulomb interactions in vacuo, the net electric charges of the ionic Arg and Glu residues were decreased to half of their initial values, while those of the N- and C-terminal charged groups were neglected. The ϕ angle for the nonglycine L-residues was constrained between −175 and 0°.

RESULTS AND DISCUSSION

Measurement of mAb Binding to the Nonphosphorylated and Phosphorylated Peptides. A direct ELISA and a competitive RIA were used. Earlier studies with Pepscan peptides (nonpurified peptides synthesized on the surface of plastic rods to which they remained attached during the binding experiments) showed that 11 mAbs bound to the consensus sequence β381−388, which contained the β-subunit tyrosine phosphorylation site (β384); this sequence is identical in *Torpedo* and human AChR.

In the first experiment, these 11 mAbs, together with the control mAb 5 (directed against the cytoplasmic region of the α-subunit), were tested in a direct ELISA for binding to immobilized *Torpedo* peptide β380−391, which contained the above consensus sequence β381−388, and to a control peptide, α67−76, containing the main immunogenic region (MIR). Figure 1 shows that six out of the 11 mAb bound well to the β-subunit peptide, while the others are characterized with weak or no binding.

The ability of the nonphosphorylated *Torpedo* and human β380−391 peptides to inhibit the binding of five of the six positive mAbs to the intact *Torpedo* AChR in solution was then tested in a competitive RIA. Figure 2 shows that the nonphosphorylated human peptide was able to inhibit the binding of all five mAbs. Similar results were also obtained with the nonphosphorylated *Torpedo* peptide (data non shown).

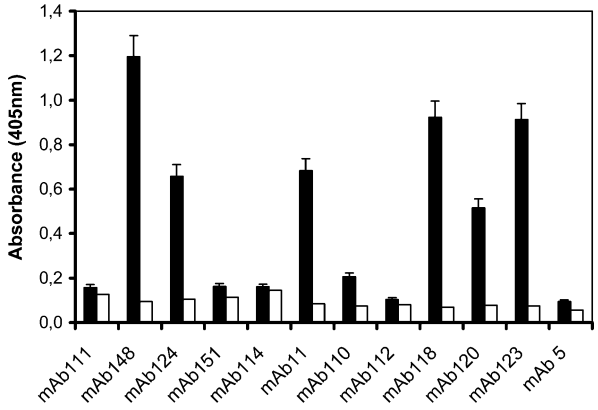

FIGURE 1: ELISA screening of a selected group of mAbs for binding to peptides corresponding to *Torpedo* AChR β380−391 (black bars) and α67−76 (spotted bars), used as a negative control. mAb 5 was used as a negative control antibody.

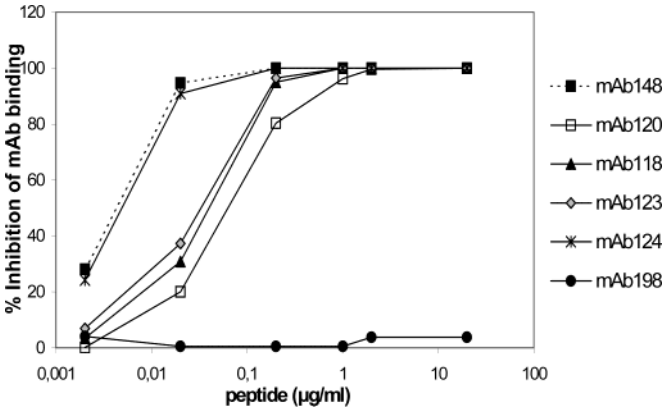

FIGURE 2: Inhibition by the nonphosphorylated human β380−391 peptide of the binding of mAbs to ^{125}I-α-bungarotoxin-labeled *Torpedo* AChR in solution. The binding of all five selected mAbs was strongly inhibited, whereas the binding of the control anti-MIR, mAb 198, was unaffected.

mAb 148 was selected for all subsequent studies for the following reasons: (i) it gave the highest binding to *Torpedo* peptide β380−391 in the ELISA experiments (Figure 1), (ii) its binding to AChR was efficiently inhibited by the soluble human nonphosphorylated β-subunit peptide (Figure 2), and (iii) it can inhibit agonist-induced channel opening (*16*, *17*). Figure 3 compares the ability of the four β380−391 peptides (phosphorylated and nonphosphorylated *Torpedo* and human peptides) to inhibit the binding of mAb 148 to the intact AChR. All four peptides were efficient inhibitors of mAb binding, although the nonphosphorylated human peptide was less effective than the three others. Control unrelated peptides had no effect (data not shown).

^{1}H NMR Analysis. For simplicity, in the figures and tables, peptide residues are numbered from one to 13 (for human peptides) or 12 (for *Torpedo* peptides). All four free peptides exhibited only a few and weak ROE or weak negative NOE connectivities for long mixing times ($\tau_m \geq 500$ ms) in aqueous solution and in the absence of mAb 148. However, the absence of NH-NH ROE or NOE correlations denoted a rather rapid exchange between different conformations. Proline cis/trans equilibrium was observed with a 50:50 ratio only in the case of the free human nonphosphorylated peptide in aqueous solution.

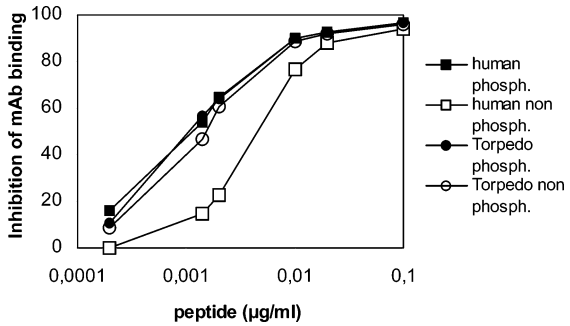

FIGURE 3: Soluble competitive RIA showing inhibition of the binding of mAb 148 to ^{125}I-α-bungarotoxin-labeled *Torpedo* AChR by the nonphosphorylated human (□) and *Torpedo* (○) and phosphorylated human (■) and *Torpedo* (●) β380−391 dodecapeptides. As a negative control, all four peptides were tested at a high peptide concentration (2 μg/mL) for their ability to block the binding of mAb 198 to the AChR, and no inhibition of binding was seen.

In previous studies, related to another antigen−antibody system (*47*), we showed that by varying the peptide/mAb molar ratio from 10 to 100, the optimal conditions for the TR-NOESY measurements were observed for a ratio near 50:1. In that study, only a few and weak negative NOEs were observed for the 10:1 peptide/mAb molar ratio. Their number and intensity increased when the peptide/mAb molar ratio reached 75:1 and then decreased at the molar ratio 100:1. To determine the structural properties of the peptides bound to mAb 148, 2-D TR-NOESY experiments were carried out on the four peptides in aqueous solution (H_2O/D_2O, 95:5, v/v, pH 7) with a mAb 148/peptide molar ratio equal to 1:50. The observation of TR-NOE cross-peaks, when mAb 148 was added, attested the peptide−antibody interaction and the restricted flexibility of the mAb-bound peptides. Because of the low mAb 148/peptide molar ratio, free and bound peptide molecules were in rapid chemical exchange, and only a single set of broadened ligand resonances was observed. The NMR signals of the four peptides in the presence of mAb 148 were attributed by the combined use of TOCSY and TR-NOESY experiments (Table S1, see Supporting Information). For all peptides, multiple TR-NOESY connectivities between side chain protons of the aromatic residues (Y_5 and F_6) and the main backbone, as well as the side chain protons of other residues, appeared upon addition of antibody suggesting that these aromatic side chains are rather frozen in the bound state.

Conformation of the Antibody-Bound Nonphosphorylated Human Peptide. As observed for the free nonphosphorylated human peptide, in the presence of mAb 148, a number of NMR signals, in particular the NH resonances, were also split into two equal components that highlight the presence of a cis/trans equilibrium at the KPP sequence. Except for the multiple connectivities of the δ and ϵ side chain protons of the Y_5 and F_6 residues with the main backbone and the side chain protons of other residues (not shown), all the NOE data used for the sequential assignment and the structure determination of the peptide in the bound state (two stereoisomers A and B) are summarized in Figure 4. A great number of NOEs were observed when the nonphosphorylated human peptide was bound to mAb 148 (Figure 4), suggesting a rather rigid conformation in the bound state. The presence of many NOEs corresponding to the aromatic protons of Y_5 and F_6 indicates that the aromatic rings were also constrained (not shown). Only the trans form of the K_9P_{10} amide bond was present [$\alpha\delta(K_9, P_{10})$ connectivity] in the complexed state, while both the cis and the trans forms of the $P_{10}P_{11}$ amide bond were observed [$\alpha\delta(P_{10}, P_{11})$ and $\alpha\alpha(P_{10}, P_{11})$ connectivities]. In this regard, the $C^{\alpha}H$/NH region of the TR-NOESY spectra suggests the occurrence of two distinct stereoisomers with correlation connectivities of almost equal intensities. It seems likely that, in the presence of mAb 148, the cis−trans ratio of the $P_{10}P_{11}$ fragment is 50:50. The absence of intense NN(i, $i + 1$) or consecutive intense αN(i, $i + 1$) NOE connectivities and medium range NN(i, $i + 2$), NN(i, $i + 3$), αN(i, $i + 2$), and αN(i, $i + 3$) NOE connectivities (Figure 4) denote the absence of secondary structures (helix, turn, or strand). Thus, both antibody-bound isomers adopt an extended structure. However, the numerous NOE connectivities observed for the side chain protons indicate that binding of the peptide by the antibody tends to freeze the rotation of the peptide side chains.

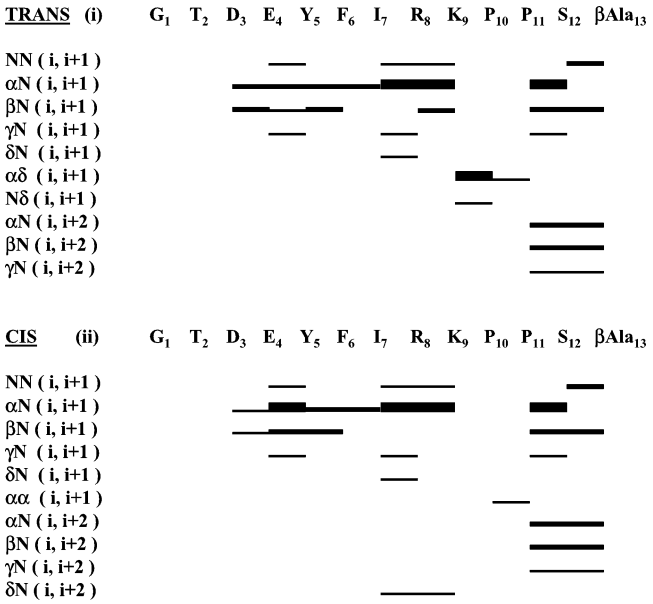

FIGURE 4: Human nonphosphorylated peptide: TR-NOE connectivities in the presence of mAb 148 (mAb/peptide molar ratio 1:50) in H_2O/D_2O, 95:5, v/v, pH 7, for trans (i) and cis (ii) P_{10}-P_{11} stereoisomers. The TR-NOE intensities are represented by different line thicknesses and are classified as strong, medium, or weak.

Conformation of the Antibody-Bound Nonphosphorylated Torpedo Peptide. In the presence of mAb 148, in contrast to the nonphosphorylated human peptide, only one set of NMR resonances was observed despite the presence of P_{10} residue. In the absence of the $\alpha\alpha(K_9, P_{10})$ connectivity, only the trans form of the K_9P_{10} amide bond appeared [presence of $\alpha\delta(K_9, P_{10})$ connectivity] in the complexed state. The TR-NOE spectrum exhibits a great number of NOEs including intense [NN(E_4, Y_5), NN(Y_5, F_6), NN(I_7, R_8)] and medium [NN(R_8, K_9), NN(A_{11}, G_{12})] NN(i, $i + 1$) connectivities suggesting the presence of secondary structures (α- or β-turns) (Figure 5). The presence of multiple NN(i, $i + 2$), αN(i, $i + 2$) and βN(i, $i + 2$) connectivities attests that the nonphosphorylated *Torpedo* peptide, in contrast to the human peptide, adopts a folded structure in the presence of mAb 148.

Conformation of the Antibody-Bound Phosphorylated Human and Torpedo Peptides. The numerous and intense TR-NOE correlations observed in the presence of mAb 148

Table 1: Averaged ϕ, Ψ, and χ_1 Values (Deg) of Restrained Molecular Dynamics Structures for the Nonphosphorylated and Phosphorylated Human (GTDEYFIRKPPS) and *Torpedo* (ANDEYFIRKPAG) Peptides in the Presence of mAb 148 in H_2O and D_2O (95:5 v/v)

		human peptide			*Torpedo* peptide		
		nonphosphorylated		phosphorylated	nonphosphorylated	phosporylated	
residue	torsion angle	trans $P_{10}P_{11}$ bond	cis $P_{10}P_{11}$ bond			family 1	family 2
G_1 or A_1	ψ	-129 ± 91	-106 ± 99	146 ± 86	122 ± 86	153 ± 79	169 ± 83
T_2 or N_2	ϕ	-108 ± 19	-103 ± 4	-109 ± 25	-106 ± 29	-89 ± 22	-92 ± 22
	ψ	95 ± 104	87 ± 8	-79 ± 53	106 ± 98	52 ± 72	66 ± 73
	χ_1	30 ± 65	56 ± 1	47 ± 66	-153 ± 85	-138 ± 79	-151 ± 76
D_3	ϕ	-101 ± 35	-91 ± 1	-106 ± 33	-48 ± 21	-53 ± 8	-58 ± 3
	ψ	-75 ± 13	-73 ± 9	170 ± 17	-38 ± 64	-34 ± 6	-49 ± 7
	χ_1	-130 ± 93	-4 ± 103	-78 ± 95	-111 ± 95	-61 ± 31	-47 ± 56
E_4	ϕ	-105 ± 13	-96 ± 2	-54 ± 5	-68 ± 34	-61 ± 1	-61 ± 1
	ψ	99 ± 7	100 ± 8	-2 ± 8	61 ± 16	-13 ± 9	-24 ± 5
	χ_1	-179 ± 2	-177 ± 1	-173 ± 67	-145 ± 43	-104 ± 60	-153 ± 69
Y_5	ϕ	-122 ± 22	-129 ± 19	-86 ± 5	-170 ± 23	-56 ± 6	-56 ± 2
	ψ	156 ± 2	156 ± 1	-19 ± 8	-61 ± 4	-46 ± 4	-18 ± 3
	χ_1	72 ± 4	70 ± 3	55 ± 65	179 ± 3	88 ± 2	-117 ± 3
F_6	ϕ	-89 ± 6	-90 ± 5	-62 ± 5	-70 ± 3	-74 ± 3	-59 ± 2
	ψ	178 ± 6	176 ± 4	-15 ± 2	-1 ± 4	-45 ± 3	-40 ± 3
	χ_1	58 ± 2	59 ± 1	80 ± 6	-72 ± 15	-169 ± 1	-171 ± 1
I_7	ϕ	-65 ± 6	-63 ± 4	-70 ± 3	-97 ± 2	-71 ± 1	-73 ± 3
	ψ	116 ± 5	120 ± 8	-29 ± 2	58 ± 5	4 ± 3	11 ± 6
	χ_1	-131 ± 24	-134 ± 15	-35 ± 4	-60 ± 2	-129 ± 2	-130 ± 3
R_8	ϕ	-111 ± 14	-99 ± 21	-141 ± 12	-94 ± 17	0 ± 4	3 ± 4
	ψ	123 ± 7	124 ± 13	-30 ± 14	104 ± 9	81 ± 5	80 ± 5
	χ_1	-66 ± 62	-78 ± 76	68 ± 47	-18 ± 54	-165 ± 18	-160 ± 17
K_9	ϕ	-118 ± 7	-122 ± 18	-129 ± 25	-124 ± 19	-87 ± 9	-86 ± 8
	ψ	102 ± 8	114 ± 16	101 ± 35	110 ± 19	120 ± 8	121 ± 8
	χ_1	-136 ± 52	-118 ± 87	-166 ± 56	-46 ± 70	-152 ± 38	-150 ± 39
P_{10}	ϕ	-72 ± 2	-75 ± 4	-70 ± 7	-70 ± 8	-74 ± 7	-69 ± 9
	ψ	128 ± 8	128 ± 3	180 ± 68	131 ± 51	97 ± 72	86 ± 76
P_{11} or A_{11}	ω	178 ± 1	-1 ± 1				
	ϕ	-78 ± 10	-74 ± 7	-73 ± 7	-136 ± 17	-102 ± 20	-106 ± 19
	ψ	150 ± 2	140 ± 5	131 ± 55	95 ± 58	80 ± 27	85 ± 17
	χ_1				165 ± 93	81 ± 92	-121 ± 104
S_{12} or G_{12}	ϕ	-67 ± 4	-66 ± 3	-104 ± 21	168 ± 44	167 ± 26	167 ± 32
	ψ	-12 ± 7	-10 ± 6	81 ± 47			
	χ_1	-63 ± 87	-95 ± 60	33 ± 91			

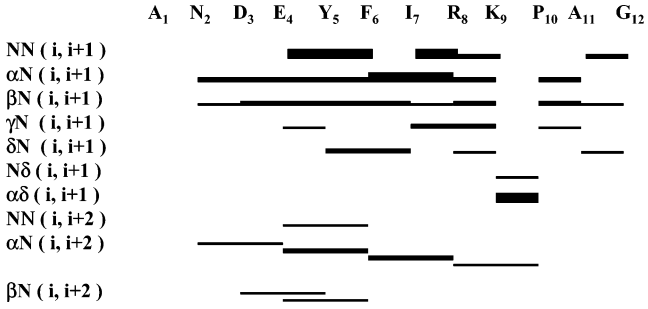

FIGURE 5: TR-NOE connectivities of the nonphosphorylated *Torpedo* peptide in the presence of mAb 148 in H_2O/D_2O 9:5, v/v, pH 7. The TR-NOE intensities are represented by different line thicknesses and are classified as strong, medium, or weak.

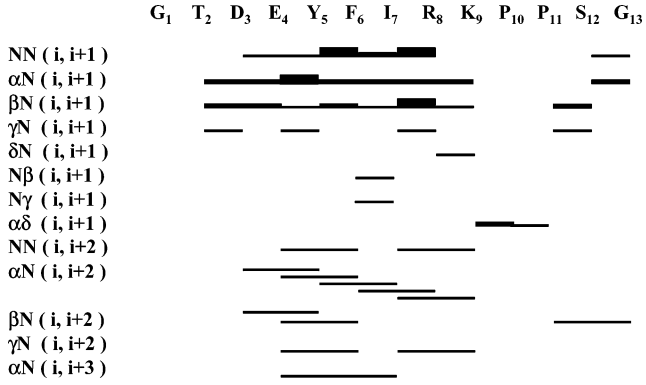

FIGURE 6: TR-NOE connectivities of the phosphorylated human peptide in the presence of mAb 148 in H_2O/D_2O 9:5, v/v, pH 7. The TR-NOE intensities are represented by different line thicknesses and are classified as strong, medium, or weak.

(Figures 6 and 7, respectively) attest a well-defined structure of the complexed phosphorylated human and *Torpedo* peptides. The NOEs corresponding to the aromatic protons (data not shown) suggest that the Y_5 and F_6 rings are strongly constrained. In contrast to the nonphosphorylated human peptide, a trans disposition was detected for both $K_9P_{10}P_{11}$ amide bonds of the phosphorylated human peptide, as confirmed by the Nδ(K_9, P_{10}), $\alpha\delta$(K_9, P_{10}), and $\alpha\delta$(P_{10}, P_{11}) NOE connectivities and by the absence of the $\alpha\alpha$(K_9, P_{10}) and $\alpha\alpha$(P_{10}, P_{11}) NOE cross-peaks. The absence of the $\alpha\alpha$(K_9, P_{10}) cross-peak and the presence of the Nδ(K_9, P_{10}) and $\alpha\delta$(K_9, P_{10}) NOE connectivities in the TR-NOESY spectrum of the phosphorylated *Torpedo* peptide indicate that the K_9P_{10} amide bond adopts also a trans disposition. The TR-NOESY spectra of the human and *Torpedo* phosphorylated peptides were quite similar. In addition to some intense NOE connectivities between successive amide protons, some medium-range NN(i, $i + 2$), αN(i, $i + 2$), βN(i, $i + 2$), γN(i, $i + 2$) and αN(i, $i + 3$) were detected for the mAb 148-bound phosphorylated peptides. These latter peaks argue in favor of a folded structure for the sequences $D_3EY(PO_3H_2)F_6$ and $Y_5(PO_3H_2)FIR_8$, which both include the Tyr phosphorylated site, whereas the αN(i, $i + 2$) consecutive

Table 2: Dimensions (Å, Deg) and Occurrence (%) of the Hydrogen Bonds[a] in Nonphosphorylated and Phosphorylated Peptides, in the Presence of mAb 148 in H_2O and D_2O (95:5 v/v), during Restrained Molecular Dynamics Simulation

				HB dimensions			HB dimensions		
donor	acceptor	hydrogen bond type	turn	distance H···O	angle <HNO	occurrence	distance H···O	angle <HNO	occurrence
				Antibody-Bound Nonphosphorylated Human Peptide					
D_3−NH	G_1−CO	$i+2 \rightarrow i$	γ^b	2.4−3.0	28−34	20			
				Antibody-Bound Nonphosphorylated *Torpedo* Peptide					
Y_5−NH	D_3−CO	$i+2 \rightarrow i$	γ^b	1.9−2.3	13−33	74			
F_6−NH	N_2−CO	$i+4 \rightarrow i$	α^c	2.0−2.8	1−21	77			
F_6−NH	D_3−CO	$i+3 \rightarrow i$		2.7−2.9	17−35	26			
R_8−NH	F_6−CO	$i+2 \rightarrow i$	γ^b	2.3−2.6	21−27	100			
				Antibody-Bound Phosphorylated Human Peptide					
Y_5−NH	D_3−CO	$i+2 \rightarrow i$	γ^b	1.9−2.2	15−25	96			
F_6−NH	D_3−CO	$i+3 \rightarrow i$	$\beta_I{}^d$	2.4−2.9	3−18	96			
R_8−NH	Y_5−CO	$i+3 \rightarrow i$	$\beta_{III}{}^d$	2.4−2.9	10−27	100			
K_9−NH	Y_5−CO	$i+4 \rightarrow i$	α^c	2.0−2.6	16−35	96			
G_{13}−NH	P_{11}−CO	$i+2 \rightarrow i$	γ^b	2.2−2.9	29−35	41			
D_3−NH	T_2−O^γ			2.2−2.3	30−35	32			
S_{12}−NH	Y_5−PO			2.4−3.7	23−28	23			
S_{12}−O^γH	P_{10}−CO			1.9−3.0	11−18	27			
				Antibody-Bound Phosphorylated *Torpedo* Peptide					
				Family 1			Family 2		
D_3−NH	A_1−CO	$i+2 \rightarrow i$	γ^b	2.4−2.7	22−35	33	2.4−2.5	24−29	29
Y_5−NH	N_2−CO	$i+3 \rightarrow i$	$\beta_{III}{}^d$	2.2−2.7	4−27	98	2.6−2.7	27−35	38
F_6−NH	D_3−CO	$i+3 \rightarrow i$	$\beta_{III}{}^d$	2.6−3.0	8−24	42	2.7−3.0	0−14	81
I_7−NH	E_4−CO	$i+3 \rightarrow i$	$\beta_{III}{}^d$				2.3−2.6	17−35	95
R_8−NH	F_6−CO	$i+2 \rightarrow i$	γ^b	2.3−2.5	24−32	100	2.2−2.5	17−33	100
G_{12}−NH	P_{10}−CO	$i+2 \rightarrow i$	γ^b	2.4−2.7	26−35	52	2.5−2.8	32−35	63
Y_5−NH	N_2−C^γO						2.3−2.9	17−32	29
A_{11}−NH	Y_5−PO						2.3−2.9	2−31	24

[a] Only the intramolecular hydrogen bonds with an occurrence exceeding 20% are indicated. [b] See ref *48*. [c] See ref *49*. [d] See ref *50*.

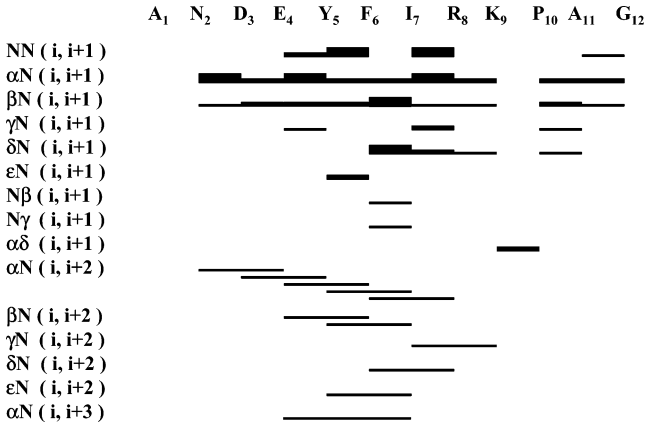

FIGURE 7: TR-NOE connectivities of the phosphorylated *Torpedo* peptide in the presence of mAb 148 in H_2O/D_2O 9:5, v/v, pH 7. The TR-NOE intensities are represented by different line thicknesses and are classified as strong, medium, or weak.

connectivities are diagnostic of a short 3_{10} helix involving the D_3EYFIR$_8$ region. It should be noted that the spatially constrained aromatic rings of Y_5 and F_6 are both incorporated within the helical part of the phosphorylated peptides.

3-D Structure Calculations. Taking into account that the measured values of the $^3J_{\alpha N}$ coupling constants correspond to the free state of the peptides, the ϕ dihedral angles, except for those of Gly, were constrained to be negative within the −175 to 0° interval. The ϕ, ψ, and χ_1 values for the averaged structures, calculated from the lowest energy retained structures (50−70 structures), are listed in Table 1. The increased or decreased flexibility of the segments may be appreciated from the magnitude of the estimated standard deviations. The dimensions (H···O hydrogen bond distance and HNO angle) and the occurrence of the hydrogen bonds were determined by using the MOLMOL software and are given in Table 2.

Human Antibody-Bound Nonphosphorylated Peptide. Two parallel calculations were performed for the two peptide stereoisomers bound to mAb 148, taking into consideration the occurrence of the trans and cis forms of the $P_{10}P_{11}$ amide bond. The best fit for the superimposed peptide backbone gave an rmsd of 0.89 ± 0.27 Å for the T_2DEYFIRKPPS$_{12}$ fragment of the human nonphosphorylated peptide, having the trans disposition of the $P_{10}P_{11}$ amide bond and an rmsd of 0.86 ± 0.37 Å for the T_2DEYFIRKP$_{10}$ fragment with the cis form of the $P_{10}P_{11}$ amide bond. Considering the cis and trans extended structures, the common TDEYFIR segments were superimposable, while the C-termini were not (Figure 8). As the two cis and trans stereoisomers are equally recognized by mAb 148 (presence of TR-NOE connectivities in both cases), at most the common superimposed TDEYFIR fragment is inside the mAb 148 binding site. The MD results (Tables 1 and 2) show that the antibody-bound nonphosphorylated human peptide adopts an extended structure. Only a 20% occurrence of the D_3-NH → G_1-CO hydrogen bonded interaction (γ-turn) was estimated.

Torpedo Antibody-Bound Nonphosphorylated Peptide. The best fit for the superimposed peptide backbone of the D_3EYFIRKP$_{10}$ fragment gave an rmsd of 0.84 ± 0.34 Å, and the averaged structure is shown in Figure 9. The structural features of the complexed nonphosphorylated *Torpedo* peptide (Tables 1 and 2) are as follows: two γ-turns around E_4 and I_7 with 74 and 100% occurrence, respectively,

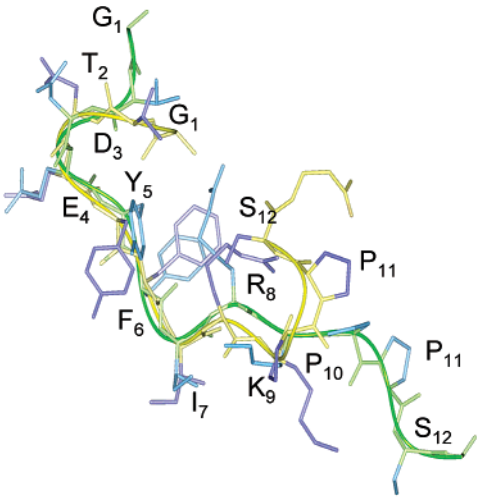

FIGURE 8: Superposition of the averaged structure of the trans (green) and cis (yellow) conformers of the human nonphosphorylated peptide in the presence of mAb 148.

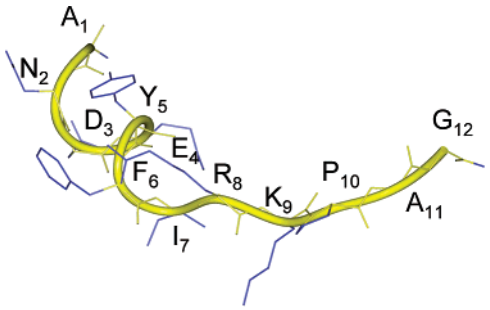

FIGURE 9: Averaged structure of the nonphosphorylated *Torpedo* peptide in the presence of mAb 148.

one α-turn with 77% occurrence of the hydrogen bonded interaction F_6-NH → N_2-CO, and finally one β-turn stabilized by the F_6-NH → D_3-CO hydrogen bond (26% occurrence). The antibody-bound peptide adopts a rather ill-defined folded structure for the calculated (ϕ_4, ψ_4) E_4 and (ϕ_5, ψ_5) Y_5 values, which are far from the classical values defining standard secondary structures.

Human Antibody-Bound Phosphorylated Peptide. The geometrical characteristics (dihedral angles ϕ, ψ, χ_1) of the complexed phosphorylated peptide as resulted from the molecular dynamics simulations are summarized in Table 1. The best fit for the superimposed peptide backbone of $D_3EY(PO_3H_2)FIRK_9$ gave an rmsd of 0.59 ± 0.28 Å, and the averaged structure is shown in Figure 10. Two γ-turns around E_4 and S_{12} were observed with 96 and 41% occurrence, respectively (Table 2). Taking into consideration the ϕ_4, ψ_4 and ϕ_5, ψ_5 dihedral angle values (Table 1), the $NH_6\cdots O_3$ distance (2.4−2.9 Å), and the occurrence (96%) of the hydrogen bonded interaction (F_6-NH → D_3-CO), we assume the presence of a β_I turn in the sequence $D_3EY(PO_3H_2)F_6$. Similarly, the ϕ_6, ψ_6 and ϕ_7, ψ_7 values, the $NH_8\cdots O_5$ distance (2.4−2.9 Å), and the occurrence (100%) of the R_8-NH → Y_5-CO hydrogen bond are in favor of a β_{III} turn in the $Y_5(PO_3H_2)FIR_8$ fragment. The hydrogen bonded interaction (K_9-NH → Y_5-CO) corresponding to an α-turn ($i + 4 \rightarrow i$) experiences 96% occurrence. Thus, these two β-turns in addition to the α-turn identified in the phosphorylated human peptide imply the formation of a compact structure when bound to mAb 148, which is

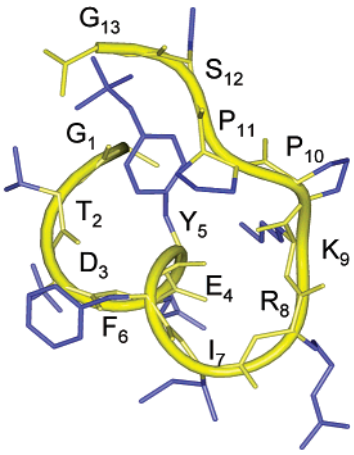

FIGURE 10: Averaged structure of the phosphorylated human peptide in the presence of mAb 148.

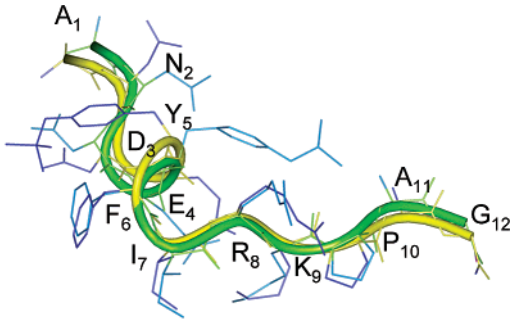

FIGURE 11: Superposition of the averaged structures (family 1 in yellow and family 2 in green) of the phosphorylated *Torpedo* peptide in the presence of mAb 148.

compatible with a distorted 3_{10} helix in the $D_3EY(PO_3H_2)$-FIR_8 region. The reported in Table 1 ϕ, ψ angles of residues E_4 (−54 ± 5, −2 ± 8°), Y_5 (−86 ± 5, −19 ± 8°), F_6 (−62 ± 5, −15 ± 2°), and I_7 (−70 ± 3, −29 ± 2°) fit better the typical values of 3_{10} helix (−49, −26°) than those of α-helix (−57, −47°).

Torpedo Antibody-Bound Phosphorylated Peptide. The NMR structural behavior of the antibody-bound phosphorylated *Torpedo* peptide is similar to that of the human peptide. Sixty-nine structures having the lowest energies were retained among the 100 initial random structures generated by using the DYANA program. The refined MD structures, using DISCOVER-3 module, were clustered into two families. The MD results are reported in Tables 1 and 2. The best fit for the superimposed peptide backbone of $D_3EY(PO_3H_2)FIRKP_{10}$ gave an rmsd of 0.47 ± 0.25 Å in the case of the first family (48 structures, 70%), 0.59 ± 0.34 Å for the second family (21 structures, 30%), and 0.73 ± 0.38 Å for the saved 69 structures. This latter rmsd value suggests that the structures of these two families are nearly the same (Figure 11). Three γ-turns around N_2, I_7, and A_{11} were found in both forms with similar occurrence (Table 2). The ϕ_3, ψ_3 and ϕ_4, ψ_4 dihedral angle values (Table 1) and the $NH_5\cdots O_2$ hydrogen bond distance (Table 2), as well as the ϕ_4, ψ_4 and ϕ_5, ψ_5 dihedral angle values (Table 1) and the $NH_6\cdots O_3$ hydrogen bond distance (Table 2) are compatible with the presence of two β_{II}-turns in each family. The occurrences of these β_{III}-turns are 98, 42% for family 1 and 38, 81% for family 2, respectively. A third β_{III}-turn, involving the I_7-NH → E_4-CO interaction, is observed in the case of family 2

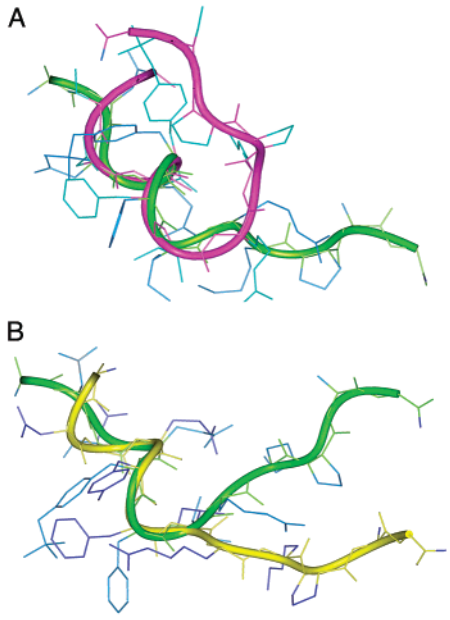

FIGURE 12: Superposition of the averaged structures of the phosphorylated *Torpedo* peptide (green) with the phosphorylated human peptide (top, purple) and with the nonphosphorylated *Torpedo* peptide (bottom, yellow) showing the best fit for the folded DEYFI segment.

with an occurrence of 95%. Two interactions between backbone amide protons and functional side chains are also detected: Y_5-NH → N_2-C$^{\gamma}$O (29% occurrence) and A_{11}-NH → Y_5-PO (24% occurrence). The main difference between the two forms originates from the $Y_5-\psi_5$ dihedral angle values (Table 1), $-46 \pm 4°$ (family 1) and $-18 \pm 3°$ (family 2). In accordance with the phosphorylated human peptide, the reported in Table 1 ϕ, ψ angles for the five residues $D_3E_4Y_5(PO_3H_2)F_6I_7$ are close to those of the standard 3_{10} helix.

The mAb 148 was chosen for its capacity to bind all four peptides. The two cis and trans stereoisomers (isomerization of the $P_{10}P_{11}$ amide bond), observed for the nonphosphorylated human peptide in aqueous solution, are equally recognized by mAb 148 (presence of TR-NOE connectivities in both cases) and adopt an extended structure in the presence of mAb 148. In this extended structure, the two Y_5 and F_6 aromatic side chains are oriented in the opposite direction. Both stereoisomers are unlikely to fit well to the antibody by their common TDEYFIR segments that are superimposed. In contrast, the nonphosphorylated *Torpedo* peptide, with all trans amide bonds, adopts a folded structure including an α-turn stabilized by the F_6-NH → N_2-CO hydrogen bond and a β-turn stabilized by the F_6-NH → D_3-CO hydrogen bond, whereas the two adjacent Y_5 and F_6 aromatic side chains are staggered. In the case of the *Torpedo* and human phosphorylated peptides, the presence of the phosphate group induces the formation of a 3_{10} helix surrounding the Y_5 residue, the phosphorylation target. Superimposition of the human and *Torpedo* phosphorylated $D_3E_4Y_5F_6I_7$ backbone atoms results in an rmsd value of 0.4 Å (Figure 12A). The helix structure, containing the F_6-NH → D_3-CO hydrogen bond, leads to a staggered disposition of the adjacent side chains including the Y_5 and F_6 aromatic side chains, as is also observed for the antibody-bound complex of the nonphosphorylated *Torpedo* peptide. Superimposition of the $D_3E_4Y_5F_6I_7$ backbone atoms of the *Torpedo* phosphorylated and nonphosphorylated peptides results in an rmsd value of 0.37 Å (Figure 12B). These two points constitute the common characteristics of the three peptides that are more effective in inhibiting the binding of mAb 148 to the AChR.

CONCLUSIONS

In this study, we demonstrated that the phosphorylated and nonphosphorylated human and *Torpedo* β380−391 AChR peptides, containing the phosphorylation site Tyr 384 of the β-subunit, efficiently inhibit the specific binding of mAb 148 to *Torpedo* AChR. However, the phosphorylated and nonphosphorylated *Torpedo* peptides, as well as the phosphorylated human peptide, are more effective than the nonphosphorylated human peptide. When complexed with mAb 148, the TDEYFIR segment of the two stereoisomers of the nonphosphorylated human peptide adopts the same superimposable extended structure, while the C-termini are not superimposable. Neither stereoisomer fits very well to the antibody as opposed to the phosphorylated peptides that were more effective in inhibiting the binding of mAb 148 to the AChR. On the other hand, the nonphosphorylated *Torpedo* peptide, which is as efficient as the phosphorylated peptides in inhibiting the binding of mAb 148 to *Torpedo* AchR, displays a rather folded structure.

When bound to mAb 148, the phosphorylated human and *Torpedo* peptides adopt a folded structure compatible with a 3_{10} helix for the DEY(PO_3H_2)FIR region, which possibly reflects the local conformation of the AChR phosphorylation site at the interface with the antibody. Our results suggest that Tyr phosphorylation induces a conformational alteration (formation of a 3_{10} helix) in the VICE-β region of AChR in the presence of mAb 148.

Since mAb 148 binds with a high affinity to the intact AChR (K_d 0.23×10^{-9} M; Tzartos, unpublished), it is reasonable to assume that the observed antibody-bound average conformation of the phosphorylated human and *Torpedo* peptides depicts the conformation of the corresponding segment in the intact phosphorylated AChR. This means that the phosphorylation of the AChR β-subunit Tyr site results in a dramatic local conformational change that could directly affect the structure of the channel, leading to a modification of the desensitization rate, and may also be responsible for other functional changes in the molecule upon phosphorylation.

ACKNOWLEDGMENT

Access to the Bruker DRX 600 NMR facilities of the Service Commun de Biophysicochimie des Interactions Moléculaires de l'Université Henri Poincaré, Nancy I, was deeply appreciated. We thank Drs. G. Boussard and M. Marraud for their critical review of the manuscript and A. Kokla for excellent technical assistance (hybridoma cultures and mAb preparation).

SUPPORTING INFORMATION AVAILABLE

Table S1: Chemical shifts (ppm) of assigned proton resonances of nonphosphorylated and phosphorylated human and *Torpedo* peptides in the presence of mAb 148 at pH 7 in H_2O and D_2O (95:5 v/v). This material is available free of charge via the Internet at http://pubs.acs.org.

REFERENCES

1. Lindstrom, J. (1996) in *Ion channels* (Narahashi T., Ed.) Vol. 4, pp 377−450, Plenum Press, New York.
2. Galzi, J. L., and Changeux, J. P. (1994) *Curr. Opin. Struct. Biol. 4*, 554−565.
3. Unwin, N. (1995) *Nature 373*, 37−43.
4. Miyazawa, A., Fujiyoshi, Y., Stowell, M., and Unwin, N. (1999) *J. Mol. Biol. 288*, 765−786.
5. Tzartos, S. J., Barkas, T., Cung, M. T., Mamalaki, A., Marraud, M., Orlewski, P., Papanastasiou, D., Sakarellos, C., Sakarellos Daitsiotis, M., Tsantili, P., and Tsikaris, V. (1998) *Immunol. Rev. 163*, 89−120.
6. Tzartos, S. J., and Remoundos, M. S. (1992) *Eur. J. Biochem. 207*, 915−922.
7. Tzartos, S. J., and Remoundos, M. (1999) *Clin. Exp. Immunol. 116*, 146−152.
8. Nestler, E. J., Walaas, S. I., and Greengard, P. (1984) *Science 225*, 1357−1364.
9. Hopfield, J. F., Tank, D. W., Greengard, P., and Huganir, R. L. (1988) *Nature 336*, 677−680.
10. Tzartos, S. J., Valcana, C., Kouvatsou, R., and Kokla, A. (1993) *EMBO J. 12*, 5141−5149.
11. Huganir, R. L., Delcour, A. H., Greengard, P., and Hess, G. P. (1986) *Nature 321*, 774−776.
12. Wallace, B. G., Qu, Z. C., and Huganir, R. L. (1991) *Neuron 6*, 869−878.
13. Ferrer-Montiel, A. V., Montal, M. S., Diaz-Munoz, M., and Montal, M. (1991) *Proc. Natl. Acad. Sci. U.S.A. 88*, 10213−10217.
14. Green, W. N., Ross, A. F., and Claudio, T. (1991) *Neuron 7*, 659−666.
15. Ferns, M., and Hall, Z. W. (1992) *Cell 70*, 1−3.
16. Lindstrom, J., Tzartos, S. J., and Gullick, W. (1981) *Ann. NY Acad. Sci. 377*, 1−19.
17. Blatt, Y., Montal, M. S., Lindstrom, J. M., and Montal, M. (1986) *J. Neurosci. 6*, 481−486.
18. Tzartos, S. J., Tzartos, E., and Tzartos, J. S. (1995) *FEBS Lett. 363*, 195−198.
19. Tzartos, S. J., Kouvatsou, R., and Tzartos, E. (1995) *Eur. J. Biochem. 228*, 463−472.
20. Clore, G. M., and Gronenborn, A. M. (1982) *J. Magn. Reson. 48*, 402−417.
21. Clore, G. M., and Gronenborn, A. M. (1983) *J. Magn. Reson. 53*, 423−448.
22. Ni, F. (1994) *Prog. NMR Spectrosc. 26*, 517−606.
23. Otting, G. (1993) *Curr. Opin. Struct. Biol. 3*, 760−768.
24. Campbell, A. P., and Sykes, B. D. (1993) *Annu. Rev. Biophys. Biomol. Struct. 22*, 99−122.
25. Anglister, J., and Naider, F. (1991) *Methods Enzymol. 203*, 228−241.
26. Rosevear, P. R., and Mildvan, A. S. (1989) *Methods Enzymol. 117*, 333−375.
27. Khosla, M. C., Smeby, R. R., and Bumpus, F. M. (1972) *J. Am. Chem. Soc. 94*, 4721−4724.
28. Rothe, M., and Mazanek, J. (1972) *Angew. Chem., Int. Ed. Engl. 11*, 293−296.
29. Stewart, J. M., and Young, J. D. (1984) in *Solid-Phase Peptide Synthesis*, Pierce Chemical Co, Rockford, IL.
30. Bodansky, M. (1993) in *Principles of Peptide Synthesis*, 2nd ed., Springer-Verlag, Berlin.
31. Bodansky, M., and Bodansky, A. (1994) in *The practice of Peptide Synthesis*, 2nd ed., Springer-Verlag, Berlin.
32. Ottinger, E. A., Shekels, L. L., Bernlohr, D. A., and Barany, G. (1993) *Biochemistry, 32*, 4354−4361.
33. Tsukamoto, M., Kato, R., Ishiguro, K., Uchida, T., and Sato, K. (1991) *Tetrahedron Lett. 32*, 7083−7086.
34. Tzartos, S. J., Langeberg, L., Hochschwender, S., Swanson, L., and Lindstrom, J. (1986) *J. Neuroimmunol. 10*, 235−253.
35. Tzartos, S. J., Kokla, A., Walgrave, S., and Conti-Tronconi, B. (1988) *Proc. Natl. Acad. Sci. U.S.A. 85*, 2899−2903.
36. Cung, M. T., Demange, P., Marraud, M., Tsikaris, V., Sakarellos, C., Papadouli, I., Kokla, A., and Tzartos, S. J. (1991) *Biopolymers 31*, 769−776.
37. Kumar, A., Wagner, G., Ernst, R. R., and Wüthrich, K. (1981) *J. Am. Chem. Soc. 103*, 3654−3658.
38. Piotto, M., Saudek, V., and Sklenar, V. (1992) *J. Biomol. NMR 2*, 661−666.
39. Sklenar, V., Piotto, M., Leppik, R., and Saudek, V. (1993) *J. Magn. Reson. 102A*, 241−245.
40. Bartels, C., Xia, T. H., Billeter, M., Güntert, P., and Wüthrich, K. (1995) *J. Biomol. NMR 5*, 1−10.
41. Güntert, P., Mumenthaler, C., and Wüthrich, K. (1997) *J. Mol. Biol. 273*, 283−298.
42. Nilges, M., Clore, G. M., and Gronenborn, A. M. (1988) *FEBS Lett. 229*, 317−324.
43. Clore, G. M., Brunger, A. T., Karplus, M., and Gronenborn, A. M. (1986) *J. Mol. Biol. 191*, 523−551.
44. Scheek, R. M., van Gusteren, W. F., and Kaptein, R. (1989) *Methods Enzymol. 177*, 204−218.
45. Koradi, R., Billeter, M., and Wüthrich, K. (1996) *J. Mol. Graphics 14*, 51−55.
46. Weiner, S. J., Kollman, P. A., Case, D. A., Singh, U. C., Ghio, C., Alagona, G., Profeta, S., Jr., and Weiner, P. (1984) *J. Am. Chem. Soc. 106*, 765−784.
47. Phan Chan Du, A., Petit, M. C., Guichard, G., Briand, J.-P., Muller, S., and Cung, M. T. (2001) *Biochemistry 40*, 5720−5727.
48. Stickle, D. F., Presta, L. G., Dill, K. A., and Rose, G. D. (1992) *J. Mol. Biol. 226*, 1143−1159.
49. Pavone, V., Gaeta, G., Lombardi, A., Nastri, F., Maglio, O., Isernia, C., and Saviano, M. (1996) *Biopolymers 38*, 705−721.
50. Rose, G. D., Gierasch, L. M., and Smith, J. A. (1985) *Adv. Protein Chem. 37*, 1−109.

BI030034U